Int J Adv Manuf Technol (2017) 89:2883–2891
DOI 10.1007/s00170-016-9751-5

ORIGINAL ARTICLE

An analytical model of grinding force based on time-varying dynamic behavior

Yinchen ma[1] · **Jianguo yang**[1] · **Beizhi li**[1] · **Jun lu**[1]

Received: 25 August 2016 / Accepted: 7 November 2016 / Published online: 26 November 2016

Abstract This paper presents a time-domain force analytical model of cylindrical grinding process, which focuses on the time-varying dynamic behaviors caused by unstable machining process. This model analyzes the dynamic behaviors between the wheel and workpiece as the contact length and the maximum undeformed chip thickness change. It contains the grinding force affected by spindle run-out and vibration and especially focuses on the variation of grinding force which is affected by grinding parameters. In order to ensure the accuracy and computational efficiency of this model, the on-line detection results of grinding process have been adopted into the force analytical model. Through this model, explanations of different grinding parameter combinations are provided for grinding mechanism observed from the simulated results. Therefore, this model is validated by comparing the simulated results with the experimental results.

Keywords Analysis model · High-speed grinding · The grinding force · The dynamic performance of the grinding process system · Process optimization

1 Introduction

In order to achieve high component quality as well as high productivity, high-speed grinding has been used as a method of precision manufacturing. Compared with the conventional speed grinding, high-speed grinding is widely employed to achieve high machining qualities and higher productivity, lower force on workpiece, and longer tool life [1–5]. However, in the view of the material formation, high-speed spindle rotation system and the thinner chips created by high-speed grinding are not the first considerations, as it leads to the unbalance of system and sophisticated the grinding mechanism. On the one hand, the increasing speed of grinding wheel can lead to the difficulties of ensuring dynamic stiffness, vibration resistance, thermal performance, and dynamic balance. On the other hand, the interface friction conditions, the flow characteristics of the materials, and the cutting speed have significant influences on the chip formation, [6] which reflect dynamic response that can affect the stability of grinding process and the grinding quality. Therefore, it is necessary to make a research about the dynamic behaviors of high-speed grinding, which observe the influences of different grinding system, grinding parameter, and machining environment. An instrumented MGKS1332/H grinding machine was used as the object to simulate the grinding process, and it has been employed to study the influences of the process parameters for the reliability and stability of high-speed grinding.

To eliminate the influence of the chip size effect, and to make the research on the speed effect of material removal mechanism, a study to understand high-speed grinding process and to provide information for grinding optimization is necessary. [7] A great deal of literatures regarding simulation model and sensor experimental analysis have been developed in order to ensure the stable grinding processes. It is believed that the grinding conditions such as the grinding wheel, the workpiece material, and the grinding parameters have a great influence on the dynamic variations of grinding force, vibration, power, etc., because of the interaction between the wheel and workpiece. Besides, it terminally affects the grinding quality. Wan M [8–11] made a research about the mechanics

✉ Yinchen ma
mayinchen@aliyun.com

[1] Mechanical Engineering School, Donghua University, Shanghai 201620, China

and dynamics of the milling process and studied on the construction mechanism of stability lobes in milling process with multiple modes. Based on the single-grit grinding, Lin T [12] studied the speed effect on the changes in material deformation and chip formation. It demonstrated that the stages of material removal process changed with the grinding speed, the graphical relationships between the grinding speed, and the critical thickness of chip formation; the grinding forces and the pile-up ratio were found to have a common characteristic, namely, a common turnover point which was about 100 m/s. The dynamic grinding force model about the empirical approaches and the methods of Guo MX [13] is the indispensable reference for grinding process stability. This work can be used to quantitatively describe the force with amplitude-frequency characteristic and facilitate the understanding of the influences of grinding parameters on dynamic performance. Jiang JL [14] proposed 3D ground surface topography models to analyze the influence of wear and dressing on grinding quality, where the number of grinding tool's grains and grinding depth vary and greatly affect the grinding quality. Except for what has been talked above, chatter is one of the most critical problems influencing the stability in the grinding process. Moreover, it affects the dimensional accuracy, surface finish, tool life, and machine reliability. It is believed that the chatter in grinding mechanism is more complicated than those in the cutting processes because of the double regenerations on both the workpiece and grinding wheel, stochastic characteristics of grinding wheels, and the significant effects of contact deformation. Inasaki I [15] discussed the chatter regenerative effects on its influence of surface quality and presented the possibilities related to process monitoring for the detection of chatter during the grinding. Altintas Y [16] presented the dynamic model and chatter stability of milling, and various stability models, which were compared against experimentally validated time-domain simulation model results. In Hahn's [17] work, the workpiece regenerative chatter has been analyzed while Snoeys and Brown [18] developed a doubly regenerative feedback loops to analyze the grinding process. Considering the regenerative loops of the grinding wheel and workpiece, some researchers have found the solutions to the chatter boundary. Thompson [19–21] presented an alternative analytical method, which is a simple harmonic normal force assumed acting on the grinding interface. Through this method, the stable boundary and the chatter growth were obtained.

The existing simulation model [22] based on the grinding mechanism in current literatures cannot explain experimental observations in high-speed grinding process. Leonesio M [23] proposed a force model, which takes into account the nonlinearity of the grinding force with respect to the cutting parameters, grinding damping effect, contact stiffness, and machine-workpiece dynamics in all the relevant degrees of freedom. Thompson RA [24] proved that the conditional stability of a plunge cylindrical grinder is worked out in explicit terms of wheel and workpiece speed. Li HQ [25–27] presented a time-domain model, which simulates cylindrical plunge grinding processes under the condition of general grinding. In his model, the distributed nonlinear force along the contact length and the geometrical interaction between the wheel and workpiece has been taken into consideration. However, some aspects of the grinding are difficult to be considered into the model, such as the spindle dynamic behavior variation at high rotational speed, where the centrifugal force on the bearings, the gyroscopic effect, and the thermal effects can change the stability of grinding process. In this paper, a new model is proposed to predict the grinding force as the function of operation parameters, and it will exactly reflect the dynamic response variation of cylindrical plunge grinding. A Matlab computer program has been developed, which can predict uncut chip thickness, forces, power, etc. The experimental observations tested by grinding machine have been carried out against the simulation model, and the simulation model can partly replace the experimental observation and explain the principles of grinding mechanism.

2 Time-domain analytical model for dynamic response of cylindrical plunge grinding processes

Time-domain model for dynamic response of high-speed cylindrical plunge grinding processes consists of seven components: the model of grinding kinematics, the contact length model between the grinding wheel and workpiece, the model of undeformed thickness, the grinding force variation based on workpiece run-out, dynamic force, instantaneous coefficients, and power and dynamic response.

As a predictive model, it describes the dynamic grinding process accurately in several critical aspects. First, high-speed grinding mechanism of plunge grinding has been considered: chip thickness of wheel and contact length between the wheel and the workpiece have been changed when the wheel spindle is running in high speed. Second, the grinding force and wheel speed variations based on workpiece run-out have been calculated because they have a great influence on grinding quality. Third, other stability effects resulted from wheel speed, uncut chip thickness, and grinding tool grits have been considered as well. In addition to that, the on-line detection results of grinding process have been adopted into the force analytical model.

2.1 Cylindrical grinding simulation model based on discretized segment kinematics

Cylindrical grinding simulation model has been used to create the dynamic response, which caused by geometrical interference between the grinding wheel and workpiece. Figure 1

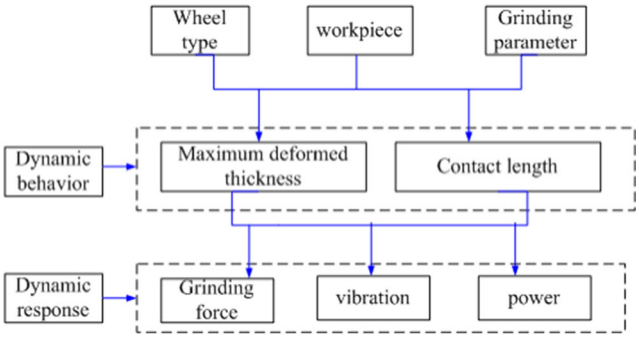

Fig. 1 Time-domain model for cylindrical grinding

shows the relationships among the grinding process parameter, dynamic behavior, dynamic response, and grinding quality. In this figure, the dynamic behaviors including uncut chip thickness and contact length between wheel and workpiece follow the selection of grinding wheel, workpiece, and grinding parameter. The dynamic behaviors determine the variation of dynamic response such as the grinding force, vibration, and power. The grinding qualities, such as roughness, residual stress, chatter mark, and grinding cracks, can be changed due to the effects of dynamic response.

For models of time-domain simulation, time is usually discretized into a number of steps, the size of which is determined by the frequencies of interest. At each time step i, the angular positions of the grinding wheel,θ_s, and the workpiece, θ_w, are represented as

$$\theta_s = t_i \cdot \Delta\theta \tag{1}$$

$$\theta_w = \theta_s \cdot \frac{n_w}{n_s} \tag{2}$$

where t_i is the time of each step i, n_w and n_s are the rotational speed of the grinding wheel and workpiece, and $\Delta\theta_s$ is the angular increment of the wheel for each time step, which can be represented as

$$\Delta\theta_s = 1/\text{step} \times 2 \times \pi \times n_s \tag{3}$$

where step is the number of increment in 1 s.

In general, plunge grinding process can be simplified to be a two-dimensional problem. Figure 2 shows the two-dimensional kinematic of the plunge grinding model; respectively, the surface speed of wheel and workpiece is *V*s and *V*w which are shown in Fig. 2. When the time is *ti* second, grinding wheel turn θ_s degrees. At that time, the maximum uncut chip thickness in each increment segment (corresponding) is a_{pd}.

2.2 Grinding mechanism and specific forms

To accurately describe the dynamic behavior in time-domain model, grinding mechanism, especially high-speed grinding mechanism, should be dissected. Some specific forms about the variation of the contact length and the maximum undeformed chip thickness will be considered, since these forms will be changed with the choice of machining systems and grinding parameter. According to Verkerk's [28] function, the variation of the contact length can be represented as

$$l_{sr} = 4.95\left(a_p * d_e\right)^{\alpha}\left(v_s/v_w\right)^{\beta}\exp\left[-0.0202\left(v_s/v_w\right)^{\gamma} * \ln a_p\right] \tag{4}$$

where

$$d_{eq} = \frac{d_s * d_w}{d_s + d_w} \tag{5}$$

is the equivalent diameter, respectively, α, β, γ is the characteristic parameters in grinding process system; these parameters can be derived from on-line detection equipment.

According to Malkin S's [29] function, the maximum undeformed chip thickness can be represented as

$$a_{gmax} = \left(\frac{3}{100 * \tan(\phi)} * \frac{V_w}{V_s} * \sqrt{a_p * d_{eq}}\right)^{\frac{1}{2}} * 1000 \tag{6}$$

where ϕ is the abrasive angle.

2.3 Dynamic unstable influences on grinding force

In high-speed grinding process, the subtle variation of vibration and workpiece run-out will affect grinding force, and the impact contact between wheel and workpiece will change the speed of spindle. These dynamic behaviors will terminally affect the product quality.

According to the effect of spindle eccentricity, workpiece run-out, and vibration, the relationship between the grinding system stability and wheel speed can be defined as the unstable coefficient k_{st} which can reflect the machining quality. The wheel speed is represented as the function of the unstable coefficient k_{st}.

$$n_s = \frac{60 * v_s}{d_s * \pi} * k_{st} \tag{7}$$

The grinding wheel contact stiffness is found to be nonlinear as it would be expected from contact mechanics, and the grinding wheel contact stiffness at t_i minutes, $k_r(t_i)$, is defined as the gradient of the normal force/defection curve,

$$k_r(t_i) = \frac{\mathrm{df}_r(t_i)}{\mathrm{dr}(t_i)} \tag{8}$$

where $\mathrm{df}_r(t_i)$ is the change of grinding force, and$\mathrm{dr}(t_i)$ is the variation of workpiece spindle run-out.

To obtain specific segment force at tangential direction, workpiece run-out will have a great influence on the tangential

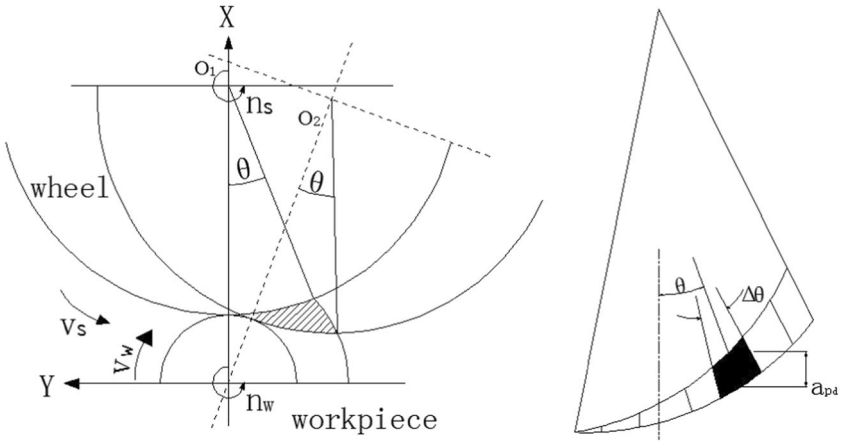

Fig. 2 Cylindrical grinding kinematics

grinding force and the renew tangential force, $f_r'(t_i)$, which can be represented as

$$f_r'(t_i) = f_r(t_i) - \int_{r(t_i-\Delta t)}^{r(t_i)} k_r(t_i) * k_0 * \mathrm{d}r(t_i) \tag{9}$$

where k_0 is the coefficient between workpiece run-out and grinding force, respectively; $f_r(t_i)$ is the basic tangential grinding force which is not affected by workpiece run-out.

2.4 Dynamic force and specific coefficient

Combined with the time-domain model method (in Parg2.1) and high-speed grinding mechanism (in Parg2.2), the dynamic grinding force is the sum of the segment force along the wheel contact length in the whole machining time, represented by

$$F_{\mathrm{sum}\_t_i} = \int_{\theta_s(t_i)-\Delta\theta(l_{sr})}^{\theta_s(t_i)} f(t_i) * d\theta_s(t_i) \tag{10}$$

where $f(t_i)$ is function of the segment force, $\theta_s(t_i)$ is wheel degree of t_i second, $\Delta\theta(l_{sr})$ is the angle of contact length.

Since the grinding process is a macro-level phenomenon, the segment dynamic force and wheel surface model are based on an average concept: average number of grits per unit area, Na, and average force per grit, f_{grit}, both of which are functions of uncut chip thickness, a_{p_d}.

To discuss the uncut chip thickness of each segment, the grinding wheel and its grits are considered as a peripheral grinding tool, respectively, based on the high-speed grinding theory; the segment instantaneous uncut chip thickness, a_{p_d}, can be approximated as

$$a_{p_d} = 2 * \pi * \frac{a_{g\max}}{N_r} * \sin\theta_s \tag{11}$$

where N_r is the number of active grits per revolution, which is related to grinding wheel surface topography.

The segment force of each contacting segment in the tangential and radial directions are represented as a function of the instantaneous uncut thickness, a_{p_d}, using the following forms similar to those of the grinding process:

$$\begin{pmatrix} f_t \\ f_r \end{pmatrix} = \begin{pmatrix} K_t \\ K_r \end{pmatrix} * a_{p_d} * N_a * A \tag{12}$$

where k_t and k_r are the specific grinding force coefficients for the tangential and radial direction, respectively, and N_aA is the total number of the active grits in the segment area, in which N_a is the number of active grits per unit area and A is the segment surface area, represented by

$$A = R_s * w * \Delta\theta_s \tag{13}$$

where R_s is the radius of the grinding wheel, and w is the grinding width.

In Eqs. (11) and (12) k_t and k_r and N_r, and N_a are the unknowns which should be received from experiments, while all the other variables can be obtained from the equations of kinematics and dynamic responses. Hence, for convenience, those unknowns are combined in the following modified forms of force coefficients to minimize the cost of experiments,

$$K_t^* = K_t \times \frac{N_a}{N_r} \tag{14}$$

$$K_r^* = K_r \times \frac{N_a}{N_r} \tag{15}$$

Thus, one can avoid the terms related to grinding wheel surface topography, N_r and N_a, which are very difficult to measure accurately in a dynamic sense. Eqs. (11) and (12) become the corresponding forms of Eqs. (16) and (17).

$$a_{p_d}^* = 2 * \pi * a_{g\max} * \sin\theta_s \tag{16}$$

$$\begin{pmatrix} f_t \\ f_r \end{pmatrix} = \begin{pmatrix} K_t^* \\ K_r^* \end{pmatrix} \times a_{p_d}^* \times A \tag{17}$$

In the next paragraph, derivations of K_t^* and K_r^* from the existing empirical static force models are presented.

2.5 Specific grinding force coefficients

K_t^* and K_r^*, specific grinding force coefficients, can be derived from an existing static force model, such as the semiempirical force model introduced by Choi and Shin [30]. The static force model right after dressing includes the effect of the grinding condition, dressing condition, and wheel size:

$$\begin{pmatrix} F_x' \\ F_y' \end{pmatrix} = \begin{pmatrix} C_x \\ C_y \end{pmatrix} * a_d^{f1} * s_d^{f2} * D_{eq}^{f3} * h_{eq}^{f4} \tag{18}$$

where C_x,C_yZ,f_1,f_2,f_3,f_4 are constant coefficients, which are obtained from typically 25–30 cylindrical grinding tests; $a_d$ands_d are the dressing depth of cut and dressing lead, respectively, D_{eq} is the equivalent diameter, represented by

$$D_{eq} = \frac{2 * R_s * R_w}{R_w \pm R_s} \tag{19}$$

and h_{eq} is the equivalent chip thickness, represented by

$$h_{eq} = \frac{v_w}{v_s} * a_p \tag{20}$$

where a_p is the depth of cut.

To obtain specific force coefficients, one needs to represent forces as a function of immersion angle, θ_i, because a relationship between the depth of cut and immersion angle can be represented as follows:

$$a_p = R_g * \left(\frac{R_g}{R_w}\right) * (1 - \cos\theta_i) \tag{21}$$

where immersion angle,θ_i, represented by

$$\theta_i = \frac{l_{sr}}{R_s} \tag{22}$$

By substituting Eqs. (19), (20), and (21) into Eq. (18), the specific grinding forces are represented as a function of immersion angle, θ_i

$$\begin{pmatrix} F_x' \\ F_y' \end{pmatrix} = \begin{pmatrix} C_x \\ C_y \end{pmatrix} * C * (1 - \cos\theta_i)^{f4} \tag{23}$$

where $C = a_d^{f1} * s_d^{f2} * D_{eq}^{f3} * \left(\frac{v_w * R_g * (R_w \pm R_g)}{v_s * R_w}\right)^{f4}$ is a constant for a given condition. Then, the specific segment forces at any angular position can be established from the derivatives of the total specific forces in Eq. (23) and setting $\theta = \theta_i$

$$\begin{aligned} \begin{pmatrix} f_x \\ f_y \end{pmatrix}_{\theta_i} &= \frac{d}{d\theta_i} \begin{pmatrix} F_x' \\ F_y' \end{pmatrix} w \Delta\theta \\ &= \begin{pmatrix} C_x \\ C_y \end{pmatrix} * C * f_4 * (1 - \cos\theta_i)^{f_4 - 1} * (\sin\theta_i) * w * \Delta\theta \end{aligned} \tag{24}$$

The specific segment forces can also be obtained by substituting f_t and $f_r$in Eq. (17)

$$\begin{pmatrix} f_x \\ f_y \end{pmatrix} = \begin{bmatrix} \cos\theta & -\sin\theta \\ \sin\theta & \cos\theta \end{bmatrix} * \begin{pmatrix} K_r^* \\ K_t^* \end{pmatrix} * a_{p_d}^* * A \tag{25}$$

After substituting the uncut chip thickness,a_{p_d}, in Eq.(7) into Eq.(21) and setting $\theta = \theta_i$, the segment forces at angular position θ_i become

$$\begin{pmatrix} f_x \\ f_y \end{pmatrix}_{\theta_i} = \begin{bmatrix} \cos\theta_i & -\sin\theta_i \\ \sin\theta_i & \cos\theta_i \end{bmatrix} * \begin{pmatrix} K_r^* \\ K_t^* \end{pmatrix} * (2 * \pi * a_{gmax} * \sin\theta_i) * (R_g * \Delta\theta) * w \tag{26}$$

By comparing the right-hand side of Eqs. (24) and (26), the specific grinding force coefficients K_r^* and K_t^*, are obtained as a function of angular position θ_i

$$\begin{pmatrix} K_r^* \\ K_t^* \end{pmatrix}_{\theta_i} = \begin{bmatrix} \cos\theta_i & \sin\theta_i \\ -\sin\theta_i & \cos\theta_i \end{bmatrix} * \begin{pmatrix} C_x \\ C_y \end{pmatrix} * \left(\frac{C * f_4 * (1 - \cos\theta_i)^{f_4 - 1}}{2 * \pi * a_{gmax} * R_g}\right) \tag{27}$$

3 The experimental results and analysis of time-domain dynamic analysis model for grinding force

The author carried out relevant research results of engineering experiment by using the high-speed cylindrical grinding machine of advanced manufacturing technology research center laboratory of Donghua University. The maximum grinding wheel spindle operating speed of this grinding machine is 9000 RPM; the diameter of grinding wheel is 0.4 m, so the highest grinding wheel linear velocity can reach 188 m/s. The grinding workpiece material used in the experiment is SiC ceramic; therefore, ceramic bond diamond wheel (D91 V 2046 j1sc-23 C150 E) was chosen as grinding wheel. Main parameters and their combination related to the grinding process shows in the Table 1.

According to multi-sensor detecting experiment, supplementary index alpha, beta, and gamma, which can be

Table 1 Constant coefficients tested by cylindrical grinding experiments

Constant coefficient	C_x	C_y	f_1	f_2	f_3	f_4
	550	35.6	−0.42	−0.22	1.39	0.85

obtained, substitute these indexes into formula (4); the contact length is obtained as

$$l_{sr} = 4.95\left(a_p{*}d_e\right)^{0.5}\left(v_s/v_w\right)^{-0.216}\exp\left[-0.0202\left(v_s/v_w\right)^{0.33}{*}\ln a_p\right] \quad (29)$$

The unstable coefficient k_{st} also can be cutting a curve with the detected data.

$$y = 1.047 + 0.1747\cos(0.6225x) - 0.4406\sin(0.6225x) \quad (30)$$

According to the typically 25–30 cylindrical grinding experiments, the constant coefficient C_x,C_y,f_1,f_2,f_3,f_4 has been calculated in Table 2.

Figure 1 shows that the dynamic time-domain prediction model, respectively, does calculation on maximum undeformed thickness, the instantaneous chip thickness, grinding thickness change, and segment grinding force; the total normal and tangential grinding force is finally got in Fig. 3. As shown in Fig. 3, the normal grinding force is equal to 25 N and the range of force within 1.0876 N. When the wheel speed is 40 m/s, the workpiece speed is 0.1 m/s and the feed is 8 μm.

According to the mentioned simulation method, the change of process parameters such as the grinding wheel speed, workpiece speed, and feed will have different grinding force results. Through observing the wheel linear velocity and its related process parameters and considering the high efficiency grinding mechanism, grinding process optimization can be developed according to the value of grinding force and its fluctuation change.

Due to the grinding wheel speed changes in simulation experiments, the change of tangential grinding force and normal grinding force can be observed in Fig.4. For instance, when grinding feed is varying from 5 to 8 μm, and grinding wheel speed increases from 40 m/s to ultra-high speed 140 m/s, the maximum tangential grinding force falls by 67%. This example shows that the grinding force and the surface roughness can be reduced by using high performance ceramic materials in grinding process. For ceramic material, under the conditions of the same material removal, the better size, shape precision, and surface organization can be obtained in low wheel speed.

In order to see into the changing rules of the tangential grinding force and normal grinding force in the condition of the constant material removal rate, Fig. 5 shows the grinding force changing rules of ceramics when the wheel speed varies from

Table 2 Relative force results in grinding process

Exp.	Wheel speed (m/s)	Depth of cut	Workpiece speed (m/s)	Normal force (RMS)	Normal force fluctuation	Tangential force (RMS)	Tangential force fluctuation
20	40	5	0.1	51.4929	4.7381	16.1473	0.4637
21	40	5	0.16	74.6485	6.9865	23.379	0.6796
22	40	8	0.1	80.6473	10.7008	25.1941	1.0558
23	40	12	0.067	84.3479	14.7685	26.6923	1.725
32	60	8	0.1	57.6769	19.8576	18.0866	2.4313
40	80	5	0.1	29.076	12.8871	9.0157	1.4244
41	80	5	0.16	42.9395	19.2623	13.3998	2.2711
42	80	8	0.1	44.7757	21.7407	14.032	3.3118
43	80	12	0.067	46.0307	22.0731	14.4857	4.5336
50	100	5	0.1	23.3799	11.6573	7.3638	1.3394
52	100	8	0.1	36.4659	20.6075	11.5101	3.3808
61	120	5	0.16	30.0702	14.1462	9.4573	1.7004
62	120	8	0.1	30.988	18.8442	9.7456	2.7967
63	120	12	0.067	31.4318	19.627	9.7369	3.7082
70	140	5	0.1	16.9686	10.0316	5.4167	1.024
71	140	5	0.16	26.0784	14.152	8.283	1.6739
72	140	8	0.1	26.4545	18.7785	8.4633	2.5992
73	140	12	0.067	26.6892	18.5091	8.384	3.4883

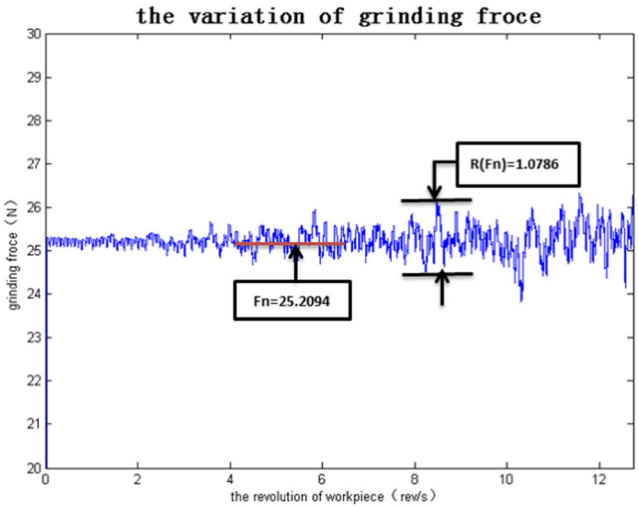

Fig. 3 Grinding force in tangential direction

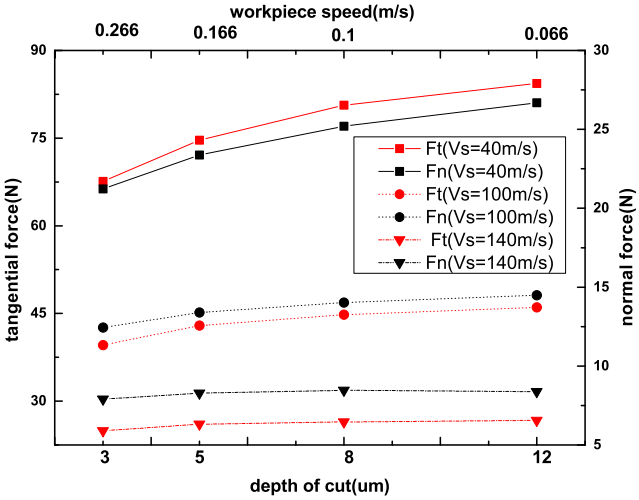

Fig. 5 The influence on the grinding force with the same material remove rate

40 to 140 m/s. In Fig. 5, with the same constant material removal rate, when the wheel speed increases, the grinding force decreases, respectively; when the wheel speed is high, the grinding force does not have big changes when workpiece speed and grinding depth change. Large linear velocity of workpiece and smaller grinding depth are conducive to reduce the grinding force and the deformation of thin-walled parts as well.

In Fig. 6, the changing rules of the normal force and its fluctuation with wheel speed can reflect the processing stability in high-speed grinding machining. When the feed is 5 μm, the workpiece speed changes from 0.1 to 0.16 m/s. Besides, the normal grinding force and its fluctuation increase. With the increase of wheel speed, the normal grinding force reduces, but the fluctuation forms a turning point, which is the largest fluctuation in the grinding wheel at the speed of 80 m/s. It shows that high-speed grinding machine tool processing and ceramic materials are the most unstable at the speed of 80 m/s.

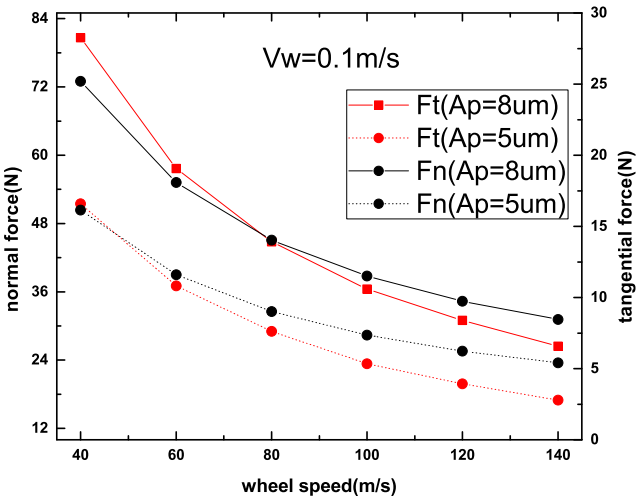

Fig. 4 Grinding force influenced by wheel speed based on the analytical model

In the view of the requirements of SiC ceramic material high quality grinding, the grinding process parameter optimization design and grinding experiment are carried out according to the grinding force regulation from Figs. 3, 4, and 5. Figure 7 shows three groups of morphology, Ra value of typical grinding process parameters and the surface roughness. In Fig. 7a, b, the grinding surface roughness can be improved by 1 or 2 level through promoting the grinding wheel's speed and reducing the grinding depth and workpiece speed. For example, Fig. 7a–c Ra0.541 corresponding to the rank of roughness standards Ra0.8, Ra0.255 corresponding to Ra0.4, and group Ra1.55 corresponding to Ra0.2.

According to the grinding force simulation from time-domain analytical force model, the simulation results are highly similar with the experimental data which detected by dynamometer sensor, and it shows the validity of the analytical model. As Fig. 8 shows, with the same material removal rate, the change of the grinding depth and workpiece speed have

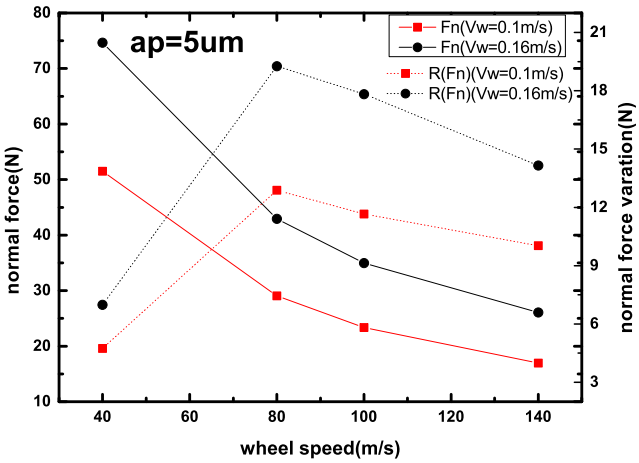

Fig. 6 Mean value and its variation of grinding force with wheel speed

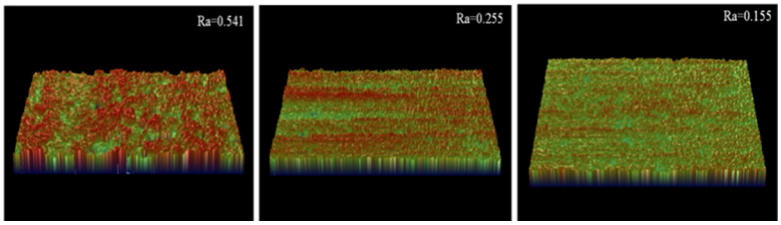

(a) vs=60m/s,vw=0.1m/s, ap=8 μ m (b) vs=80m/s, vw=0.1m/s, ap=3 μ m (c) vs=140m/s,vw=0.05m/s, ap=1 μ m

Fig. 7 Grinding process parameter optimization design results considering the working performance and its surface roughness. **a** vs = 60 m/s, vw = 0.1 m/s, ap = 8 μm. **b** vs = 80 m/s, vw = 0.1 m/s, ap = 3 μm. **c** vs = 140 m/s, vw = 0.05 m/s, ap = 1 μm

the same influence on the grinding force. The experimental results are similar to the predictive results, but the grinding force is small when the grinding feed is 3 μm. The reason of the small force is that the grinding process is more stable when the grinding depth is small. As Fig. 9 shows, with the increase of wheel speed, the normal force falls by 80% and the largest fluctuation in the grinding wheel at the speed of 80 m/s. The experimental results are similar to the analytical model results, and the predictive error is less than 10%.

4 Conclusion

Comprehensively considering the grinding force of the grinding conditions such as grinding process parameters, the morphology of grinding wheel, grinding wheel run-out, and the dynamic behavior of workpiece spindle, a time-domain dynamic analytical model of the grinding force is constructed. By using the tool of MATLAB and programming, the complex and tedious calculation work can be completed quickly. After a lot of calculations and analyses, the summarized grinding regulation is matched with the existing research results of the grinding mechanism.

The dynamic analytical model differs from the existing model in several critical aspects. First, this model analyzes the dynamic behaviors between the wheel and workpiece as the contact length and the maximum undeformed chip thickness change. Second, the grinding force and wheel speed variations based on workpiece run-out have been calculated because they have a great influence on grinding quality. Third, other stability effects resulted by wheel speed, uncut chip thickness, and grinding tool grits have been considered as well. Except that the on-line detection results of grinding process have been adopted into the force analytical model. The validity of the analytical model and its above-mentioned optimization design method are verified through the further grinding test. Comparing with the simulation and the test method, the analytical model has ultra-high efficiency and accuracy in the optimization design process.

The obtained characteristic parameter of actual grinding process system based on the multi-sensor-detection and fusion processing can modify the time-domain dynamic analysis model of the grinding force and possess better practicability and universality. Illustrated by the experiment and engineering application, the accuracy results can be simulated from the dynamic analytical model. The predictive results are similar to the experimental results, and the predictive error is less than 10%.

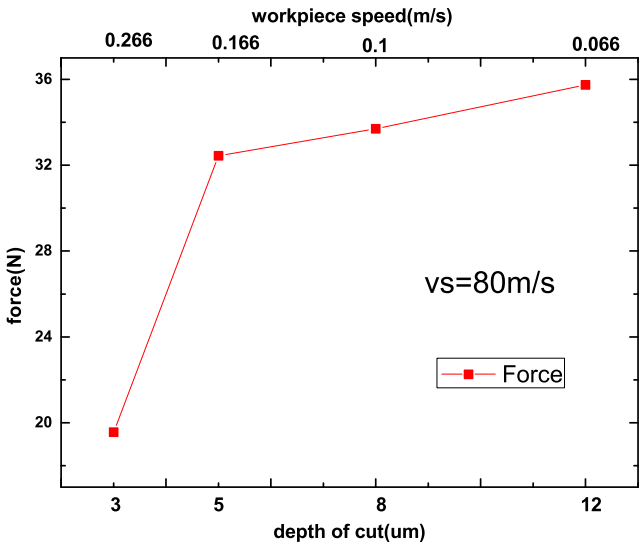

Fig. 8 The influence on the grinding force with the same material remove rate (grinding force detected by sensor)

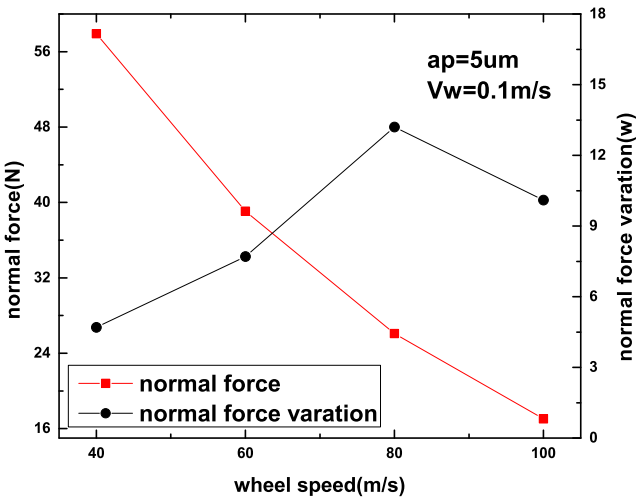

Fig. 9 Mean value and its variation of grinding force with wheel speed (grinding force detected by sensor)

Acknowledgements The authors gratefully wish to acknowledge the support of The National Natural Science Fund, China (No.51675096) and the Innovation Fund of Central University (13D310302).

References

1. Hwang TW, Evans CJ, Malkin S (2000) An investigation of high speed grinding with electroplated diamond wheels. CIRP Ann Manuf Technol 49(1):245–248
2. Jackson MJ, Davis CJ, Hitchiner MP, Mills B (2001) High speed grinding with CBN grinding wheels—applications and future technology. J Mater Process Technol 110(1):78–88
3. Ha MK, Kwak JS, Hwang YM, Chung JS (2004) Machining characteristics of mold material in high-speed grinding. J Mater Process Technol 155:1189–1195
4. Schulz H, Moriwaki T (1992) High-speed machining. CIRP Ann Manuf Technol 41(2):637–643
5. Kopac J, Krajnik P (2006) High-performance grinding—a review. J Mater Process Tech 175:278–284
6. Jackson MJ, Davis CJ, Hitchiner MP, Mills B (2001) High-speed grinding with CBN grinding wheels Ð applications and future technology. J Mater Process Tech 110:78–88
7. Li B, Ni J, Yang J, Liang SY (2014) Study on high-speed grinding mechanisms for quality and process efficiency. Int J Adv Manuf Technol 70(5):813–819
8. Wan M, Ma YC, Wei JZ, Zhang H (2016) Study of static and dynamic ploughing mechanisms by establishing generalized model with static milling forces. Int J Mech Sci 114:120–131
9. Wan M, Altintas Y (2014) Mechanics and dynamics of thread milling process. Int J Mach Tool Manu 87:16–26
10. Wan M, Kilic ZM, Altintas Y (2015) Mechanics and dynamics of multi-functional tools. Trans ASME J Manuf Sci Eng 137(1): 011019
11. Wan M, Ma YC, Wei JZ, Yang Y (2015) Study on the construction mechanism of stability lobes in milling process with multiple modes. Int J Adv Manuf Technol 79:589–603
12. Lin T, Huang H, Ramesh K, Huang T (2005) High speed versus conventional grinding in high removal rate machining of alumina and alumina–titania. Mach Tools Manuf 45:897–907
13. Guo MX, Li BZ, Ding ZS, Liang S (2016) Empirical modeling of dynamic grinding force based on process analysis. Int J Adv Manuf Technol 1–11
14. Jiang JL, Ge PQ, Bi WB, Zhang L, Wang DX (2013) 2D/3D ground surface topography modeling considering dressing and wear effects in grinding process. Int J Mach Tool Manu 74(74):29–40
15. Inasaki I, Karpuschewski B, Lee HS (2001) Grinding chatter-origin and suppression. CIRP Ann Manuf Technol 50(2):515–534
16. Altintas Y, Weck M (2004) Chatter stability of metal cutting and grinding. CIRP Ann Manuf Technol 53(2):619–652
17. Hahn RS (1954) On the theory of regenerative chatter in precision-grinding operations. Trans ASME 76(1):593–597
18. Thompson RA (1977) On the doubly regenerative stability of a grinder: the combined effect of wheel and workpiece speed. ASME J Eng Ind 99:237–241
19. Rowe WB (2009) Principles of modern grinding technology. William Andrew Press, Norwich
20. Thompson RA (1986) On the doubly regenerative stability of a grinder: the theory of chatter growth. ASME J Eng Ind 108:75–82
21. Thompson RA (1992) On the doubly regenerative stability of a grinder: the effect of contact stiffness and wave filtering. ASME J Eng Ind 114:53–60
22. Shimizu J, Zhou LB, Eda H (2002) Simulation and experimental analysis of super high-speed grinding of ductile material. J Mater Process Technol 129:19–24
23. Leonesio M, Parenti P, Cassinari A et al (2012) A time-domain surface grinding model for dynamic simulation. Procedia CIRP 4: 166–171
24. Thompson RA (1977) On the doubly regenerative stability of a grinder: the combined effect of wheel and workpiece speed. J Eng Ind 99(1):237–241
25. Li HQ, Yun CS (2005) A time-domain dynamic model for chatter prediction of cylindrical plungle grinding processes. J Manuf Sci E-T ASME 128(2):404–415
26. Li HQ, Yun CS (2007) A study on chatter boundaries of cylindrical plungle grinding with process condition-dependent dynamics. Int J Mach Tool Manu 47:1563–1572
27. Nakajima T, Yoshikawa M, Tsukamoto S, Takehara K (1998) Simulation of ground surface profile generation with measured distribution of mounting spring constant, dimensional position and shape of abrasive grains. Jap Soc Precision Eng 64(7):1072–1077
28. Verkerk J, Pekelharing AJ (1975) The real contact length in cylindrical plunge grinding. CIRP Annal 24(1):259–264
29. Malkin S, Guo C (1989) Grinding technology: theory and applications of machining with abrasives[M]. Industrial Press Inc, USA
30. Choi T, Shin YC (2007) Generalized intelligent grinding advisory system. Int J ProdRes 45(8):1899–1932